Fast-responding pressure-sensitive paints for unsteady flow measurements

Masaharu Kameda[1,*]

[1]Department of Mechanical Systems Engineering, Tokyo University of Agriculture and Technology, Koganei, Tokyo 184-8588, Japan
[*]corresponding author: kame@cc.tuat.ac.jp

Abstract Recent topics in unsteady pressure measurements using the fast-responding pressure-sensitive paints (PSP) are presented. The PSP is a luminescent paint for determining surface pressure distribution by measuring changes in the intensity of emitted light. The fast-responding PSPs developed in last decade have a rise time of 1 μs, and are utilized for measuring the pressure fluctuation whose amplitude less than 100 Pa. Progress in the formulation and characterization of the paint, and the application to unsteady phenomena such as buffet on a delta wing in a transonic flow and trailing edge noise of NACA0012 wing in low-speed flow are presented.
Keywords: Pressure-sensitive paint, Unsteady flow, Wind tunnel test

1 Introduction

Pressure-sensitive paint (PSP) is now widely used in wind tunnel testing[1, 2]. The PSP is an luminescent coatings in which oxygen-sensitive dyes are supported by binding materials. The PSP can serve us surface pressure distribution on the body on which the PSP is coated, with using a light source for exciting the dyes and a camera for detecting the luminescence emitted from the dyes. The PSP is applicable to measurement of the pressure on sharp-edges, small models, and rotating models, on which it is difficult to place conventional pressure taps.

Fast-responding pressure-sensitive paints (fast-responding PSP) is a state-of-the-art technique developing rapidly in the 21st century, especially in the U.S. and Japan. The fast-responding PSP has short rise time, usually within 1 ms. A special fast-responding PSP achieved the rise time in the order of 1 μs. This fast-responding characteristics enable us to detect the unsteady pressure due to aerodynamic sound, and the shock wave propagating along the model. Owing to rapid improvement in high-speed imaging technology, small-amplitude pressure fluctuation observed in low-speed flow can be captured by the fast-responding PSP. Nice reviews on recent progress in fast-responding PSP measurements are available[3, 4].

In this paper, recent progress in fast-responding PSP's technology is presented: development and characterization of the paints and application to wind tunnel test.

2 Response mechanism

The principle of the PSP is based on oxygen-quenched luminescence of special molecules[1, 2]. The molecules in electrically exited states return to their ground state by one of several mechanisms including emission of luminescence and dynamic quenching. The dynamic quenching results from collisions between the molecules and quencher. Oxygen is a typical quencher. The lifetime of excited molecules strongly depends on the concentration of oxygen. This principle can be applied to measure the pressure in air, because the concentration of oxygen in air is proportional to pressure.

Since the lifetime of sensor molecules for pressure-sensitive paints is typically less than 10 μs, the PSP is suitable for measuring unsteady pressure fluctuation with high frequencies. However, the temporal response of quenching is restricted severely by the permeation process of the quencher (oxygen) in the PSP. The PSP consists of the sensor molecules contained in a transparent oxygen-permeable binder. Thus, the collisional quenching occurs only when the molecules interact with the oxygen permeated into the binder by diffusion process.

In this section, a mathematical model for dynamic response of PSP[5] is introduced. The model includes both the effects of diffusion in the binder and photochemical kinetics.

2.1 Gas diffusion

Gas permeation into thin film like PSP can be characterized using one-dimensional diffusion process in which the characteristic time of diffusion is

$$\tau_D = \frac{h^2}{D}, \tag{1}$$

where h and D denote film thickness and gas diffusivity in the film.

We assume the film has an open end ($z = 0$) and a closed end ($z = h$). The concentration of the gas (oxygen) changes periodically at the open end. In this case, a general solution for the concentration is described as[6]

$$n(z',t') = \sum_{m=0}^{\infty} \alpha_m(t') \cos\left(\lambda_m z'\right) + F(t'), \qquad \lambda_m = \left(m + \frac{1}{2}\right)\pi. \tag{2}$$

with

$$n(z',0) = n_0, \tag{3}$$

$$n(1,t') = n_0 + \Delta n \sin\left(\omega\tau_D\right) t' \equiv F(t') \quad (t' > 0), \tag{4}$$

$$\frac{\partial n(0,t')}{\partial z'} = 0, \tag{5}$$

where t' and z' denote nondimensional time and distance normalized by τ_D and h. n_0 denotes undisturbed concentration. Δn and ω are the amplitude and angular frequency of the concentration fluctuation.

The amplitude for the mode m (α_m) is readily obtained from the diffusion equation[5, 7]:

$$\alpha_m(t') = -\Delta n \frac{2\sin\lambda_m}{\lambda_m} \frac{\omega\tau_D}{\sqrt{\lambda_m^4 + \left(\omega\tau_D\right)^2}} \cos\left(\omega\tau_D t' - \delta_m\right), \qquad \delta_m = \tan^{-1}\left(\frac{\omega\tau_D}{\lambda_m^2}\right). \tag{6}$$

2.2 Photochemical kinetics

The rate of luminescence intensity $e_L(t)$ can be described as a function of time with a first-order ordinary differential equation[1],

$$\frac{de_L}{dt} + \frac{e_L}{\tau_L} = E(t), \tag{7}$$

where $E(t)$ denotes the rate of absorption of photons that produce luminescence, and τ_L the lifetime of an exited dye. When we consider the radiationless deactivation and the dynamic quenching associated with the emission of luminescence, the lifetime τ_L is given by

$$\frac{1}{\tau_L} = k_E + k_T + k_Q, \tag{8}$$

where k_E, k_T, and k_Q are the rate constants for luminescence, radiationless deactivation, and dynamic quenching, respectively. k_Q is linearly proportional to the concentration of quencher (in this case, equivalent to air pressure p)

$$k_Q = k_Q' p, \tag{9}$$

where k_Q' is the proportionality factor.

First, we consider the situation that the lifetime is much smaller than the characteristic time of pressure fluctuation with a constant illumination $E(t) = E_0$. Since the time derivative in Eq. (7) can vanish in this case, the emission rate e_L is

$$e_L = E_0\tau_L. \tag{10}$$

With using the emission rate e_{L0} at a reference pressure p_0,

$$e_{L0} = E_0 \tau_{L0}, \qquad \tau_{L0} = \frac{1}{k_E + k_T + k'_Q p_0}, \tag{11}$$

we obtain the well-known Stern-Volmer equation for the ratio of e_{L0} to e_L:

$$\frac{e_{L0}}{e_L} = \frac{\tau_{L0}}{\tau_L} = \frac{k_E + k_T + k'_Q p}{k_E + k_T + k'_Q p_0} = b + (1-b)\frac{p}{p_0}, \qquad b = \frac{k_E + k_T}{k_E + k_T + k'_Q p_0}. \tag{12}$$

Note that the lifetime at the reference condition τ_{L0} and pressure sensitivity $1-b$ can be measured by calibration. Therefore, we can determine the sum of rate constants $k_E + k_T$, and the proportional factor k'_Q as

$$k_E + k_T = \frac{b}{\tau_{L0}}, \qquad k'_Q = \frac{1-b}{\tau_{L0} p_0}. \tag{13}$$

Next, we consider the situation that the lifetime is not so small as the characteristic time of pressure fluctuation. The rate of luminescence e_L for small-amplitude sinusoidal pressure fluctuation $p = p_0 + \varepsilon \exp(i\omega t)$ is

$$\frac{de_L}{dt} + \left[k_0 + k'_Q \varepsilon \exp(i\omega t)\right] e_L = E_0, \tag{14}$$

where $k_0 = k_E + k_L + k'_Q p_0$. Periodic solution for Eq. (14) would be[5]

$$e_L = e_{L0}\left[1 - \frac{1 - i\omega\tau_{L0}}{1 + (\omega\tau_{L0})^2}(1-b)\frac{\varepsilon}{p_0}\exp(i\omega t)\right]. \tag{15}$$

2.3 PSP working equation

Using Eq. (15) with Eqs. (2) and (6), we readily obtain the intensity at the nondimensional time t' and position z'[5] as

$$\begin{aligned}\frac{I(z',t')}{I_0(z')} &= 1 - (1-b)\frac{\Delta p}{p_0}\frac{1}{\sqrt{1+(\omega\tau_{L0})^2}} \times \left\{ \left[1 - \sum_{m=0}^{\infty} \frac{2\sin\lambda_m}{\lambda_m} \frac{\omega\tau_D}{\sqrt{\lambda_m^4 + (\omega\tau_D)^2}} \sin\delta_m \right] \sin\left(\omega\tau_D t' - \delta_{L0}\right) \right. \\ &\left. - \sum_{m=0}^{\infty} \frac{2\sin\lambda_m}{\lambda_m} \left(\frac{\omega\tau_D}{\sqrt{\lambda_m^4 + (\omega\tau_D)^2}} \cos\delta_m \right) \cos\left(\omega\tau_D t' - \delta_{L0}\right) \right\},\end{aligned} \tag{16}$$

where Δp is the amplitude of pressure at the surface of PSP, and $I_0(z')$ is the average intensity at the position z'. The phase difference δ_{L0} is

$$\delta_{L0} = \tan^{-1}(\omega\tau_{L0}). \tag{17}$$

Overall intensity of PSP film $\bar{I}(t')$ is

$$\bar{I}(t') = \int_0^1 I(z',t')dz', \tag{18}$$

where we assume that the average intensity $I_0(z')$ is constant irrespective of the position, which implicitly means uniform distribution of luminophore as well as no attenuation of light through the film.

Finally, using the Stern-Volmer equation (12), the pressure determined by the PSP signal $\bar{p}(t')$ can be calculated by

$$\frac{\bar{p}(t')}{p_{\mathrm{ref}}} = \frac{1}{1-b}\left[\frac{I_{\mathrm{ref}}}{\bar{I}(t')} - b\right], \tag{19}$$

where I_{ref} denotes the overall intensity at the reference pressure $p_{\mathrm{ref}}(= p_0)$.

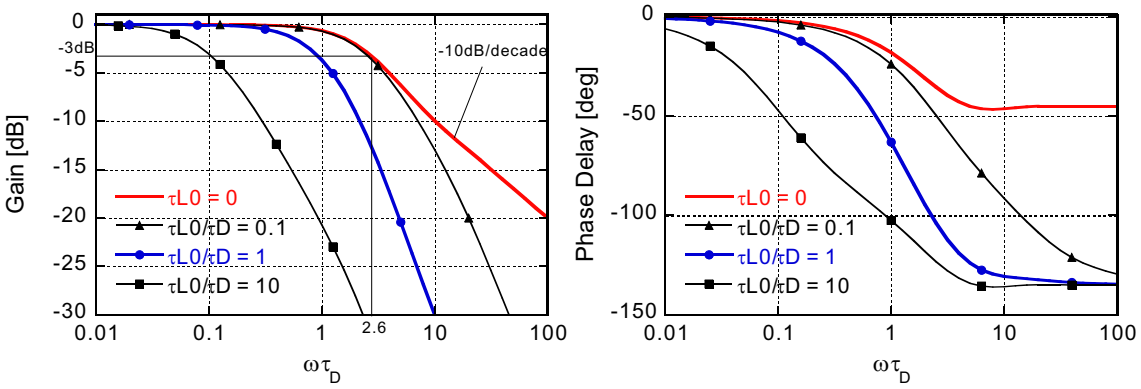

Fig. 1 Bode plot of PSP response.

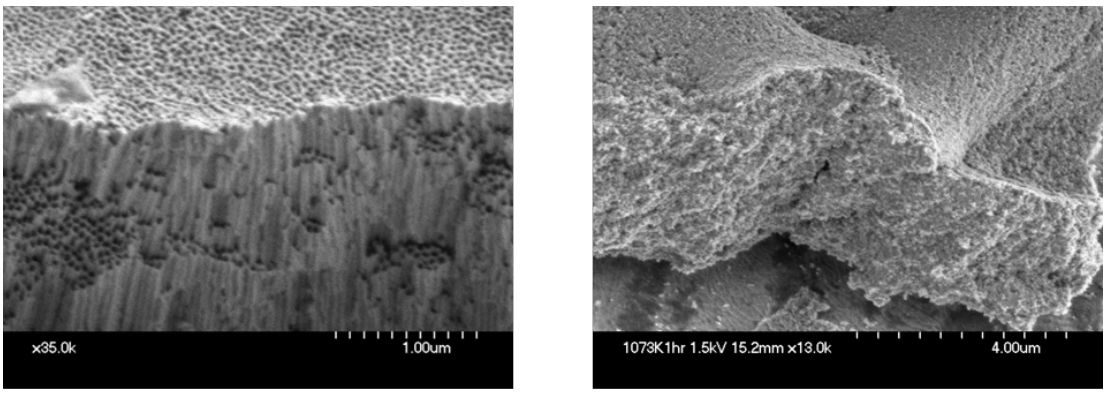

Fig. 2 FE-SEM images of porous binder. (a) anodized aluminum[13], (b) silica nanoparticle[20]

2.4 Bode plot

A Bode plot for the PSP signal is shown in Fig. 1. We plot 4 curves for the values of the ratio $\tau_{L0}/\tau_D = 0$, 0.1, 1, and 10. The constant b in Eq. (12) is 0.2.

Figure 1 indicates that the lifetime of luminescence hardly affects the frequency response of the PSP signal unless the ratio τ_{L0}/τ_D is greater than 0.1.

The case where $\tau_{L0} = 0$ agrees well with the diffusion theory for the PSP signal by Winslow et al.[7], in which the gain

$$\text{Gain} = 20\log_{10}\frac{\Delta\bar{p}}{\Delta p}, \tag{20}$$

decays -10 dB/decade at $\omega\tau_D \gg 1$, and the phase difference ϕ converges $-45°$. The characteristic time of diffusion τ_D can be experimentally defined using the cut-off frequency (-3dB) f_C: $\tau_D \simeq 0.4/f_C$.

On the contrary, in the case where $\tau_{L0}/\tau_D = 10$, the slope of the gain at $\omega\tau_{L0} > 1$ ($\omega\tau_D > 0.1$) is approximately -20 dB/decade, and the phase difference at $\omega\tau_{L0} = 1$ is $-45°$. These are typical characteristics in first-order lag system:

$$\text{Gain(lifetime)} = -10\log_{10}\left[1+(\omega\tau_{L0})^2\right], \quad \phi\text{(lifetime)} = -\tan^{-1}(\omega\tau_{L0}). \tag{21}$$

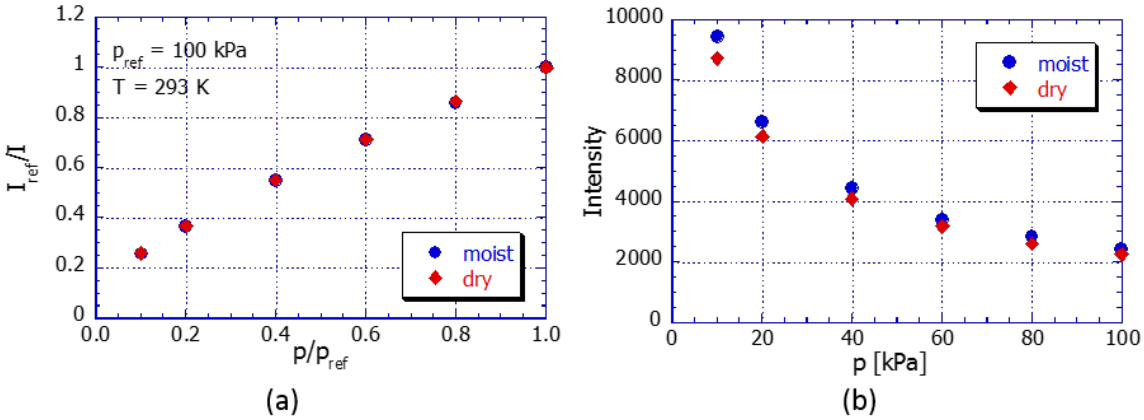

Fig. 3 Pressure sensitivity of AA-PSP[13]. (a) Stern-Volmer plot. (b) Intensity versus pressure. The temperature was 293 K. Vapor pressure in the moist air was 1.15 kPa (50% RH (relative humidity) at 293 K). The light source was a 300-W Xenon lamp with an optical bandpass filter whose transmission wavelength was 460±50 nm. The detector was a 14-bit cooled charge-coupled device (CCD) camera with an optical bandpass filter whose transmission wavelength was 650±50 nm.

3 Paint development

As mentioned in section 2, the time response of PSP is characterized by the time constant for gas diffusion τ_D as well as the lifetime of excited dye τ_L. The lifetime of common pressure-sensitive dyes at atmospheric pressure is about 8 μs for tetra(pentafluorophenyl)porphyrin (PtTFPP) and 0.08 μs for tris(4,7-diphenyl-1,10-phenanthroline) ruthenium(II)dichloride ($[Ru(dpp)_3]Cl_2$)[8].

Common polymer paint has the gas diffusion of $O(10^{-9})$ m^2/s and the thickness of 10 μm[1], so that the diffusion time scale τ_D exceeds 0.1 s, which is much larger than the lifetime of the dye. In order to reduce the diffusion time scale, several attempts have been made to find a new binder having a much larger diffusion coefficient. The "porous" material is a key to achieve the goal, because it is much easier for oxygen to permeate into such a porous material than into pure solid materials like polymer.

Several porous pressure-sensitive paints have been developed last two decades. Among them, two porous PSPs are commonly used in practical purpose: anodized-aluminum PSP and polymer/ceramic PSP.

3.1 Anodized-aluminum PSP

Anodized aluminum PSP (AA-PSP) was originally developed by Asai et al.[9]. Later Sakaue and co-workers[10, 11] improved its performance by revision of fabrication process. The anodized aluminum layer is a porous material, in which there are huge numbers of highly ordered micropores with uniform diameter and spacing (see Fig. 2(a)). The luminophore is adsorbed on the surface of anodized aluminum.

The AA-PSP having 20-nm-diameter of pores and 10 μm of thickness is commonly used in practical purpose[13, 14], Owing to its large size of pores, the gas diffusion coefficient D of the AA-PSP is estimated to be larger than 10^{-6} m^2/s[12], so that the diffusion time scale τ_D is less than 100 μs. According to the diffusion theory described in previous section, the cut-off frequency is expected to be larger than 4 kHz, which was confirmed by resonance tube tests[8, 15].

The diffusion coefficient increases as the diameter of pore becomes large[12]. The AA-PSP having 100-nm-diameter of pores and a few μm of thickness was applied to detect reflections and diffractions of shock waves[16] in which the shock waves having rise time of approximately 1 μs was successfully captured.

Typical static characteristics of AA-PSP are displayed in Fig. 3[13]. The intensity of luminescence under a continuous excitation. The intensity-pressure relation at room temperature was calibrated for dry and moist conditions. These relations were tested using a calibration chamber. Figure 3(a) and (b) indicate the Stern-Volmer and the intensity-pressure plots, respectively. The reference intensity I_{ref} in Fig. 3(a) was defined as the

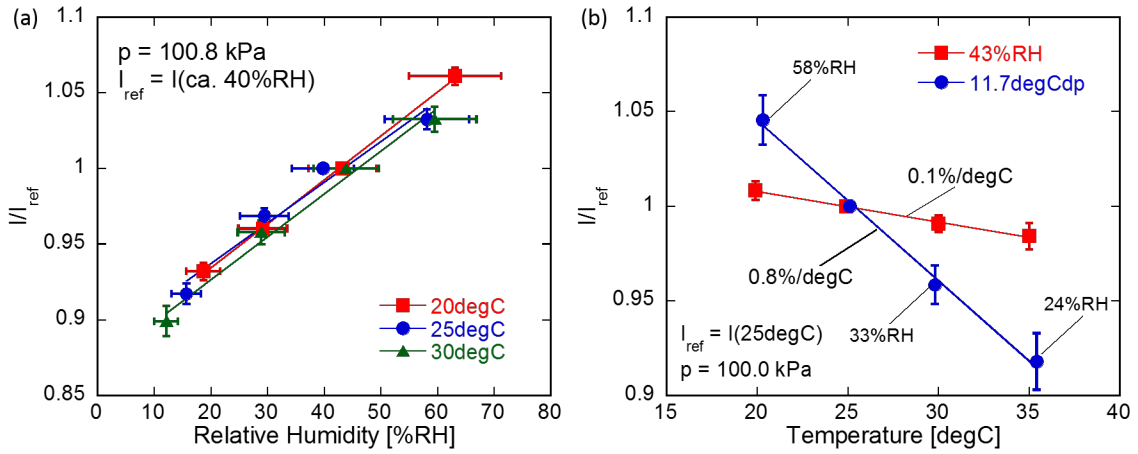

Fig. 4 Humidity- and temperature sensitivities of AA-PSP[18]. (a) Humidity sensitivity for different constant temperatures, (b) Temperature sensitivity at a constant dew point (blue symbols) and at a constant relative humidity (red symbols).

intensity at p_{ref} = 100 kPa. The slope of relative intensity (I_{ref}/I) for the moist air was the same as that for the dry air. The value approximately 0.6%/kPa is equivalent to that for conventional polymer PSP. The intensity for the moist air, on the other hand, was larger than that for the dry air.

In room temperature condition, the surface of the metal oxides without special surface modification exhibits hydrophilic nature due to chemically adsorbed hydroxyl group onto the surface. Especially, the anodized alumina contains a certain amount of electrolyte anions[17]. Therefore porous metal oxides are effective absorbents of moisture in air. In order to evaluate the effect of humidity on the emission characteristics in detail, we newly equipped a calibration apparatus, in which pressure, temperature and humidity can be controlled independently[18].

Intensity change due to difference in relative humidity is shown in Fig. 4(a)[18]. The intensity is normalized by the value at about 40%RH at each temperature. The intensity increases as the relative humidity increases as shown in Fig. 3. Notice that the slope of normalized intensity is a constant value of about 0.28%/%RH irrespective of temperature. This implies that the amount of residual water plays an important role in humidity sensitivity of AA-PSP. Residual water in the anodized alumina increases as the relative humidity increases. The energy exchange between oxygen and the luminophores covered by water molecules may be reduced because oxygen molecules are hard to interact with the luminophores.

The temperature sensitivity is shown in Fig. 4(b)[18]. We plotted the relative intensity for various values of temperature at a constant dew point of 11.7°C, which had the same meaning as the constant moisture content. The reference temperature was 25°C. Another line of data was plotted for various values of temperature at a constant relative humidity of 43%RH, because the moist air whose dew point is 11.7°C had the relative humidity of 43%RH at 25°C.

The slope of the line with a constant moisture content was 0.8%/°C, which was much larger than the slope with a constant relative humidity (0.1%/°C). The relative humidity of the test air at a constant moisture content decreases as the temperature rises due to increase of the saturated vapor pressure. For example, the relative humidity at 20°C of 58%RH is 34%RH larger than the relative humidity at 35°C as displayed in Fig. 4(b). Thus, the intensity change due to difference in temperature at a constant moisture content is the sum of the intensity change due to difference in temperature alone and the intensity change due to difference in relative humidity.

3.2 Polymer/ceramic and similar sprayable PSP

Although it has several advantages such as large pressure-sensitivity, good photostability, and hardness of the coated surface, AA-PSP is limited to be formed on aluminum surface, which casts a shadow in the application of

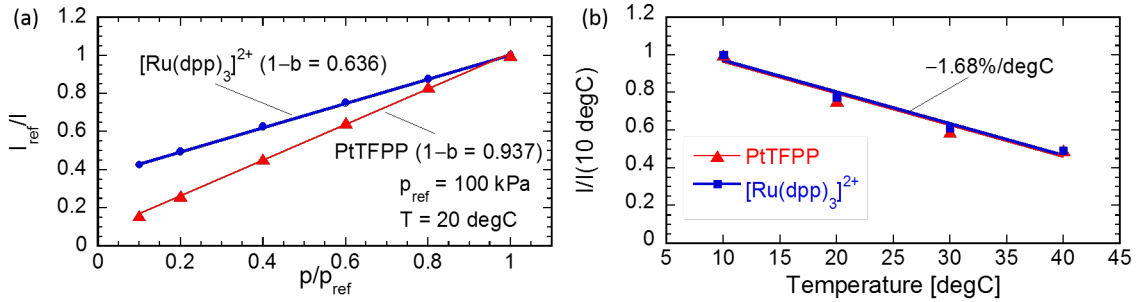

Fig. 5 (a) Pressure- and (b) temperature sensitivities of silica nanoparticle PSP[20].

the paint. Sprayable paints similar to polymer-based paints are required in order to be free from the restriction of surface materials. Gregory et al.[3] developed a sprayable fast-responding PSP called polymer/ceramic PSP (PC-PSP), which was preliminary developed by Scroggin et al.[19] using a tape casting procedure. The PC-PSP uses a binder containing ceramic (typically TiO_2) particles with a a small amount of polymer. The luminophore is applied by mixing it within the binder solution and by dipping deposition or overspraying on the polymer/ceramic surface.

We developed another sprayable paints using silica nanoparticles (silica nanoparticle PSP)[20], whose slurry can form a film on the surface without additive of polymer (see Fig. 2(b)).

The pressure- and temperature sensitivities of the silica nanoparticle PSP are shown in Fig. 5[20]. The pressure-intensity relation (Fig. 5(a)) was measured at a constant temperature of 20 °C. The pressure sensitivity exhibits a linear Stern-Volmer relation in terms of pressure [Eq. (7)]. The slope factor $1-b$ estimated by curve fit is 0.937 (%/kPa) for PtTFPP and 0.636 (%/kPa) for $[Ru(dpp)_3]^{2+}$. Difference in the slop factor between two dyes is probably caused by difference in the permeability of the silica nanoparticle film. The hydrophobic nature of PtTFPP may cause the large permeability of the film, which enhances the rate of oxygen quenching ($k'_Q \rightarrow$ large).

The silica nanoparticle PSP have larger temperature sensitivity than AA-PSP, as shown in Fig. 5(b). The slope is $-1.68\%/°C$ for films with both dyes, which is close to that for a conventional PSP.

4 Applications

Fast-responding PSP has been applied in wide range of unsteady flows. The applications from early stage until now are observation of shock waves (e.g. [16]), flow around a body with shock waves[13, 21, 22], fluidic oscillators[23], and flow in a nozzle[14, 24]. Recently, the application is spread into rotating blades[25] and vortex shedding from a square cylinder[26]. Here two examples of the applications our group and a collaborator are introduced: buffet on a delta wing in transonic flow[27] and trailing edge noise of NACA0012 wing in low-speed flow[15, 28].

4.1 Buffet

The first example is the unsteady pressure distribution on the delta wing measured by silica nanoparticle PSP. The flow over a delta wing at high angles-of-attack is dominated by two large leading-edge vortices. The vortices undergo a sudden expansion known as vortex breakdown due to adverse pressure gradient outside the vortex core. The flow downstream of the vortex breakdown is unsteady. This phenomenon is a kind of *buffet*, which is defined as the unsteady aerodynamic phenomenon involving flow separation. The vortex breakdown process is particularly complex in a transonic flow regime because of the existence of a shock wave. The complex shock-wave/vortex interaction induces “non-periodic” movement of vortex breakdown position.

Figure 6(a) shows the schematic diagram of the wind-tunnel test. The wind tunnel test was carried out with the transonic wind tunnel at ISAS of Japan Aerospace Exploration Agency (JAXA). The cross sectional area of test section is 600 mm $\times$ 600 mm. The schematic of delta wing model is shown in Fig. 6(b) with the locations

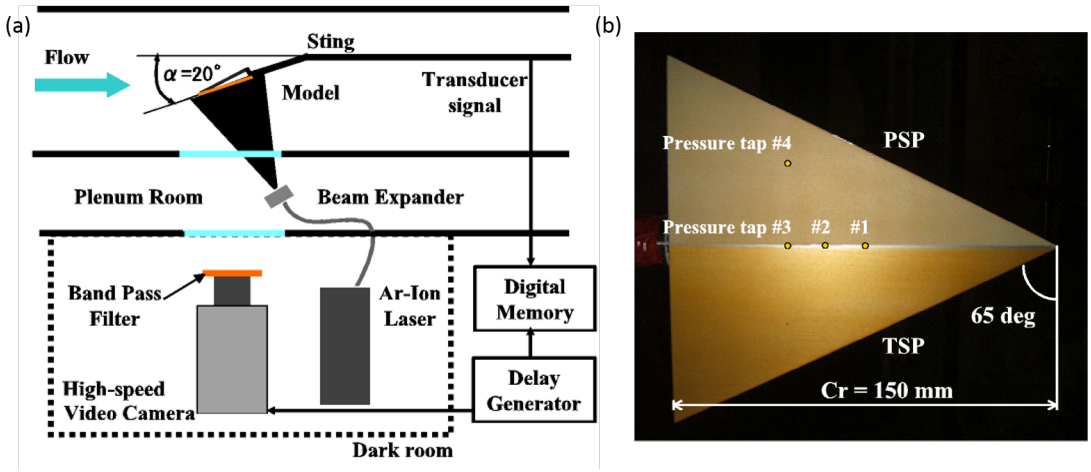

Fig. 6 Experimental setup for buffet measurement[27]. (a) Schematic of experimental apparatus. (b) Delta wing model. The luminescence on the delta wing model was observed using a 14-bit CMOS high-speed video camera (Vision Research Phantom V7.3) The delta wing model was illuminated with a 6-W Argon-ion laser. Four semiconductor-pressure transducers (Kulite XCQ-062-25A) were placed on the delta wing model. Their positions are indicated by the circles #1–#4. The output of four semiconductor-pressure transducers placed on the delta wing model was stored in a digital memory. The start timing for measuring of these measurement instruments were controlled by a 4 ch delay generator.

of semiconductor-pressure transducers. The model had 65° sweep, no camber, 150-mm-root chord (C_r), and sharp leading-edge. The silica nanoparticle PSP was applied to the starboard side of the wing. Additionally, a temperature-sensitive paint (TSP) was applied to the port side of the wing, because the temperature distribution was needed to compensate for the temperature effect of the PSP signal.

Figures 7 show some instantaneous profiles of pressure field on the delta wing in the case where $M = 0.9$. Substantial non-uniform distribution is found in pressure. High-pressure region is observed along the center axis. Pressure reduction area due to leading-edge vortices is also found in the pressure field. The pressure field on the wing surface is highly unsteady. A couple of sudden pressure rises always exists along the center axis, which are corresponding to the first and second terminating shock waves, respectively. The first terminating shock induces the vortex breakdown, which yields the pressure rise downstream the breakdown point close to the leading edge.

The pressure-time history measured by the silica nanoparticle PSP was compared with the pressure transducers as shown in Fig. 8. The PSP data represents the spatially averaged data around each pressure tap (2 pixels $\times$ 2 pixels = 0.9 mm $\times$ 0.9 mm). The pressure-time histories of PSP measurement agrees quantitatively well with the Kulite transducers within the accuracy of O(1 kPa).

4.2 Trailing edge noise

Nakakita[15, 28] applied AA-PSP to detect an unsteady pressure field with trailing-edge noise on a two-dimensional NACA0012 airfoil.

As represented by an unsteady pressure fluctuation in low-speed flow, amplitude of the pressure fluctuation is so small as below 1 kPa. Time-resolved unsteady PSP measurement described in previous subsection is difficult to be applied to such a case from the viewpoint of signal-to-noise ratio (SNR) of current high-speed video camera. If the phenomena has some dominant frequencies, phase-locked approach or frequency-domain average using fast-Fourier transform (FFT) is able to be applied to improve SNR of the PSP signal.

Figure 9 shows schematic diagram of experiment. Pressure fluctuation field on a NACA0012 model was measured at the test condition of $U = 28.0$ m/s flow speed and the model angle of attack of $-1.5°$, which was accompanied a trailing-edge noise whose fundamental frequency was around 920 Hz.

Figure 10 shows measurement results of the Kulite pressure transducer at the centerline of the 90% code ($x/c = 0.9$, $y/c = 0$). Measurement setup was 20 kHz data sampling and number of the sampling was 200 k

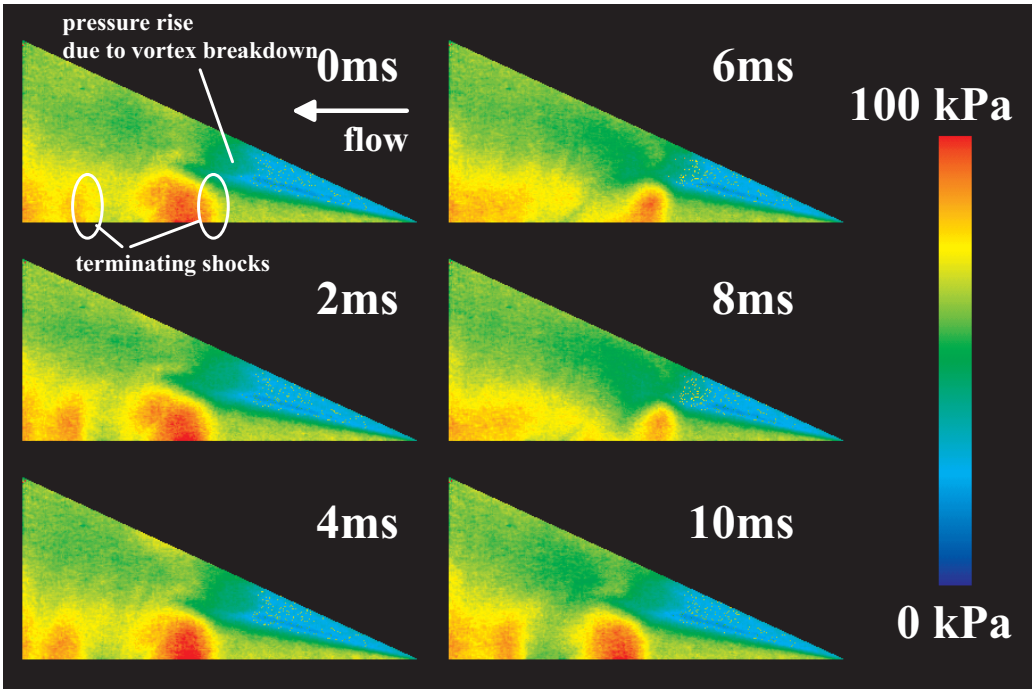

Fig. 7 Snapshots of pressure distribution at $M = 0.9$ [27]. The elapsed time was counted from the beginning of the photographing.

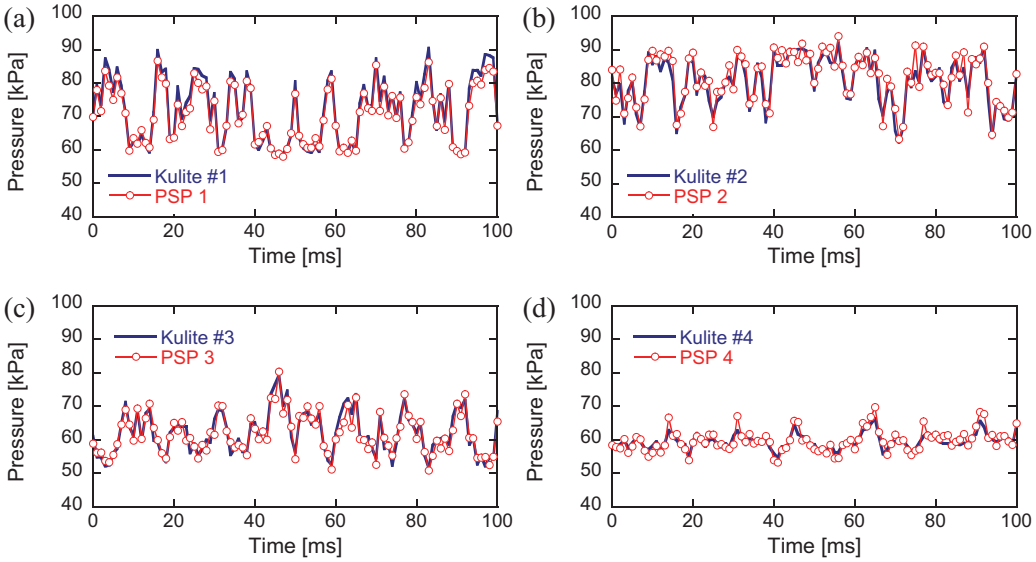

Fig. 8 Comparison of pressure-time history between Kulite and PSP at $M = 0.9$ [27].

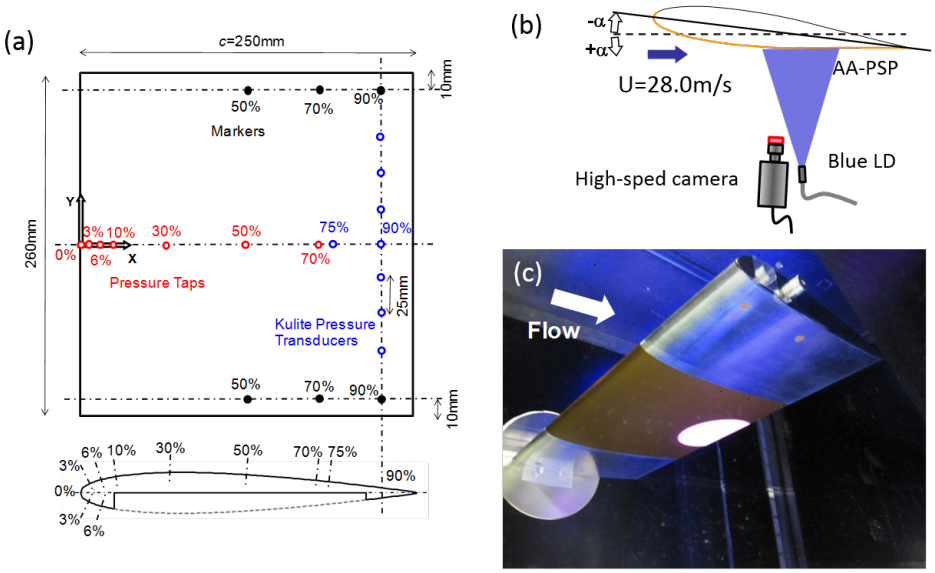

Fig. 9 Experimental setup for trailing edge noise measurement[15, 28]. (a) Outline drawing of PSP measurement part. (b) Schematic diagram of optical setup. A high-speed camera (Vision Research Phantom V710, 1280×800 pixels, 12bit) and a blue laser-diode (Sumitomo Electric BLM-7000-H08D, 7W) were placed to observe pressure side of the airfoil ($\alpha < 0$). The framing conditions were 10 kfps, 408×432 pixels of imaging area, and 53745 sequential images taken per each run. 53745 images of wind-off condition and 886 dark images were taken subsequently. (c) Illuminated model. The diameter of illuminating area was 115 mm.

points. Figure 10(a) is time-series pressure fluctuation. Its magnitude of the pressure fluctuation was about 150 Pa peak-to-peak. Figure 10(b) is the power spectrum of Fig. 10(a). Fundamental component of the unsteady pressure fluctuation was appeared at 920 Hz. Strouhal number for 920 Hz was $St = 0.985$ for wing maximum thickness 30 mm. It was a nearly pure tonal peak caused by the acoustic feedback between sound wave emitted from the trailing edge and T-S (Tollmien-Schlichting) waves on the pressure side of the airfoil. Broadband component at the bottom of the tonal peak at 920 Hz was the trailing-edge noise and the tonal peak component was grown by the selective feedback process.

Figure 11 shows the experimental results after image processing of PSP image data. Spatial distribution of (a) power, (c) coherence, and (d) phase are displayed with (b) comparison of the power calculated from PSP data with those measured by Kulite transducers.

Pressure fluctuation distribution by PSP data in Fig. 11(b) agrees well with the data by Kulite transducers. Typical discrepancy of high-speed camera unsteady PSP results from reference Kulite one was within 10 Pa owing to average over large number of images.

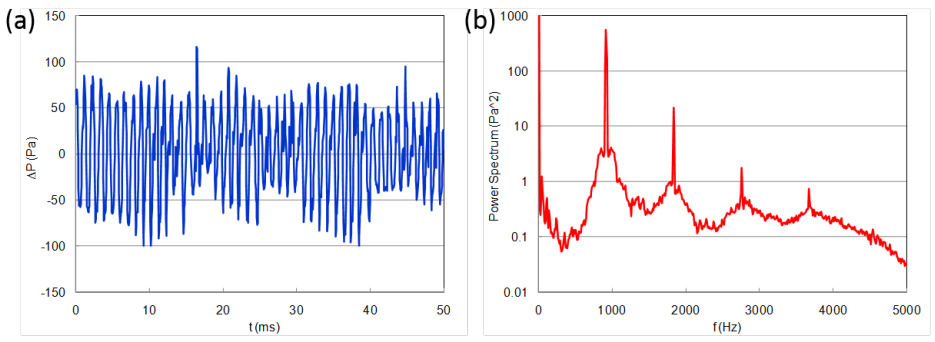

Fig. 10 Unsteady pressure measurement result by a Kulite pressure transducer[28]. (a) time-series pressure fluctuation, (b) power spectrum. $U = 28.0$ m/s, $\alpha = -1.5°$, x/c=0.9 and y/c=0.

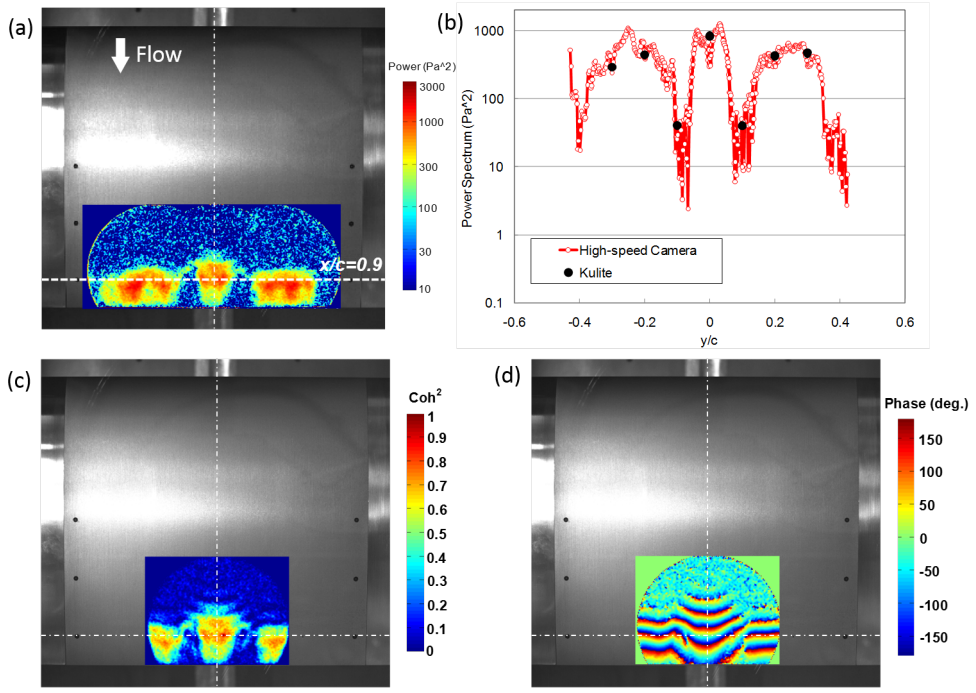

Fig. 11 Spatial distribution of various quantities[15, 28]. (a) Power (b) Comparison of pressure fluctuation distribution at 90% code ($x/c = 0.9$), (c) Coherence, (d) Phase. The experimental conditions are the same as in Fig. 10

The map of various values provides us insight to understand complicated fluid phenomena. The power is the integrated value between 918±20 Hz. Large unsteady power region appeared near the trailing edge. The power distribution exhibits three-dimensional structure nevertheless the two-dimensional model was used.

The coherence shown in Fig. 11(c) is calculated as

$$Coh^2(f) = \frac{|S_{XY}(f)|^2}{S_{XX}(f)S_{YY}(f)}, \tag{22}$$

where f is the frequency of interest, and S_{XY} is the cross-spectrum function between the unsteady pressure at two locations X and Y. S_{XX} and S_{YY} are auto-spectrum functions at X and Y. Coh^2 ranges from 0 to unity. Larger value of Coh^2 means larger correlation. Coherence map shown in Fig. 11 indicates that three regions with large power equally have large correlation $Coh^2 > 0.5$ even if their distribution looks discontinuous. Coherence between two regions might be zero if the structure of pressure fluctuation were fully individual.

5 Summary and outlook

Recent topics on fast-responding pressure-sensitive paints were presented.

The theory indicates that the frequency response of fast-responding PSP is limited by the time scale of diffusion and the lifetime of exited molecules. The diffution time scale is dominant in usual. Porous binders are used to overcome the limitation of diffusion. Anodized aluminum PSP and polymer/ceramic PSP are used in common research. Their performance is characterized well: that shows sufficiently large pressure-sensitivity similar to conventional polymer-based PSP.

The paint has been applied to wide range of flow phenomena. Non-periodic pressure fluctuation due to buffet was successfully captured by time-resolved PSP measurement with accuracy of a few kPa. With the aid of average over large number of images in frequency domain, periodic pressure fluctuation due to trailing edge noise was measured with uncertainty of O(10 Pa).

Fast-responding pressure-sensitive paint is a promised tool in common wind tunnel test such as car aerodynamics. To achieve this goal, further improvement is needed in reduction of signal-to-noise ratio of high-speed camera, light source, and luminescent intensity of the paint itself.

Acknowledgement

This work is supported by a JSPS Grant-in-Aid for Scientific Research KAKENHI (No. 25289029). The author expresses his gratitude to Prof. Keisuke Asai, Mr. Kazuyuki Nakakita and Prof. Yutaka Amao for their cooperation throughout the period of his PSP research. The author expresses his thank to K. Nakakita again who permitted using his figure in this literature. Help in experiments by several students at TUAT is greatly appreciated.

References

[1] Bell J H, Schairer E T, Hand L A, Mehta R D (2001) Surface pressure measurements using luminescent coatings, *Annual Review of Fluid Mechanics*, vol. 33, pp. 155–206. doi: 10.1146/annurev.fluid.33.1.155

[2] Liu T, Sullivan J P (2005) Pressure and Temperature Sensitive Paints. Springer, Berlin

[3] Gregory J W, Asai K, Kameda M, Liu T, Sullivan J P (2008) A review of pressure-sensitive paint for high-speed and unsteady aerodynamics, *Proceedings of the Institution of Mechanical Engineers, Part G: Journal of Aerospace Engineering*, vol. 222, pp. 249-290. doi:10.1243/09544100JAERO243

[4] Gregory J W, Sakaue H, Liu T, Sullivan J P (2014) Fast pressure-sensitive paint for flow and acoustic diagnostics, *Annual Review of Fluid Mechanics* vol. 46, pp. 303–330. doi: 10.1146/annurev-fluid-010313-141304

[5] Kameda M (2012) Effect of luminescence lifetime on the frequency response of fast-response pressure-sensitive paints, *Transactions of the Japan Society of Mechanical Engineers Series B*, vol. 78, pp. 1942–1950. doi: 10.1299/kikaib.78.1942

[6] Bird R B, Stewart W E, Lightfoot E N (2002) Transport Phenomena, 2nd ed. John Wiley & Sons, New York.

[7] Winslow N A, Carroll B F, Kurdila A J (2001) Model development and analysis of the dynamics of pressure-sensitive paints *AIAA Journal* vol. 39, pp. 660–666. doi: 10.2514/2.1359

[8] Sugimoto T, Kitashima S, Numata D, Nagai H, Asai K (2012) Characterization of frequency response of pressure-sensitive paints, In: Proceedings of 50th AIAA Aerospace Sciences Meeting Proceedings including the New Horizons Forum and Aerospace Exposition, AIAA-2012-1185. doi: 10.2514/6.2012-1185

[9] Asai K, Kanda H, Cunningham C T, Erausquin R, and Sullivan J P (1997) Surface pressure measurements in a cryogenic wind tunnel by using luminescent coatings, In: Instrumentation in Aerospace Simulation Facilities, 1997. ICIASF '97 Record, pp. 105–14. doi: 10.1109/ICIASF.1997.644671

[10] Sakaue H and Sullivan J P (2001) Time response of anodized aluminum pressure-sensitive paint, *AIAA Journal* vol. 39, pp. 1944–1949. doi: 10.2514/2.1184

[11] Sakaue H, Tabei T, Kameda M (2006) Hydrophobic monolayer coating on anodized aluminum pressure-sensitive paint, *Sensors and Actuators B* vol. 119, pp. 504-511. doi: 10.1016/j.snb.2006.01.010

[12] Kameda M, Tezuka N, Hangai T, Asai K, Nakakita K, Amao M (2004) Adsorptive pressure-sensitive coatings on porous anodized aluminum, *Measurement Science and Technology* vol. 15, pp. 489-500. doi:10.1088/0957-0233/15/3/001

[13] Kameda M, Tabei T, Nakakita K, Sakaue H, Asai K (2005) Image measurements of unsteady pressure fluctuation by a pressure-sensitive coating on porous anodized aluminum, *Measurement Science and Technology* vol. 16, pp. 2517-2524. doi:10.1088/0957-0233/16/12/017

[14] Merienne M -C, Coponet D, Luyssen J -M (2012) Transient pressure-sensitive-paint investigation in a nozzle, *AIAA Journal* vol. 50, pp. 1453–1461. doi: 10.2514/1.J050926

[15] Nakakita K (2011) Unsteady pressure measurement on NACA0012 model using global low-speed unsteady PSP technique, In: Proceedings of 41st AIAA Fluid Dynamics Conference and Exhibit, AIAA-2011-3901. doi: 10.2514/6.2011-3901

[16] Fujii S, Numata D, Nagai H, Asai K (2013) Development of ultrafast-response anodized-aluminum pressure-sensitive paints, In: Proceedings of 51st AIAA Aerospace Sciences Meeting including the New Horizons Forum and Aerospace Exposition, AIAA-2013-485. doi: 10.2514/6.2013-485

[17] Thompson G E, Wood G C (1981) Porous anodic film formation on aluminium, *Nature* vol. 290, pp. 230–232. doi:10.1038/290230a0

[18] Kameda M, Yoshida M, Sekiya T, Nakakita K (2015) Humidity effects in the response of a porous pressure-sensitive paint, *Sensors and Actuators B: Chemical* vol. 208, pp. 399-405. doi:10.1016/j.snb.2014.11.052

[19] Scroggin A M, Slamovich E B, Crafton J W, Lachendro N, Sullivan J P (1999) Porous polymer/ceramic composites for luminescence-based temperature and pressure measurements In: Materials Research Society Symposium Proceedings, vol. 560, pp. 347–352. doi: 10.1557/PROC-560-347

[20] Kameda M, Seki H, Makoshi T, Amao Y, Nakakita K (2012) A fast-response pressure sensor based on a dye-adsorbed silica nanoparticle film, *Sensors and Actuators B: Chemical*, vol. 171-172, pp. 343-349. doi: 10.1016/j.snb.2012.04.049

[21] Nakakita K, Asai K (2002) Pressure-sensitive paint application to a wing-body model in a hypersonic shock tunnel. In: Proceedings of the 22nd AIAA Aerodynamic Measurement Technology and Ground Testing Conference, AIAA 2002-2911. doi: 10.2514/6.2002-2911

[22] Bitter M, Hara T, Hain R, Yorita D, Asai K, Kähler C J (2012) Characterization of pressure dynamics in an axisymmetric separating/reattaching flow using fast-responding pressure-sensitive paint, *Experiments in Fluids*, vol. 53, pp. 1737–1749. doi: 10.1007/s00348-012-1380-7

[23] Gregory J W, Sullivan J P, and Raghu S (2005) Visualization of jet mixing in a fluidic oscillator, *Journal of Visualization*, vol. 8, pp. 169?176. doi: 10.1007/BF03181660

[24] Sakamura Y, Matsumoto M, Suzuki T (2005) High frame-rate imaging of surface pressure distribution using a porous pressure-sensitive paint, *Measurement Science and Technology*, vol. 16, pp. 759?765. doi:10.1088/0957-0233/16/3/019

[25] Disotell K J, Peng D, Juliano T J, Gregory J W, Crafton J W, Komerath N M (2014) Single-shot temperature- and pressure-sensitive paint measurements on an unsteady helicopter blade, *Experiments in Fluids*, vol. 55, 1671 (15pp). doi: 10.1007/s00348-014-1671-2

[26] Pastuhoff M, Yorita D, Asai K, Alfredsson P H (2013) Enhancing the signal-to-noise ratio of pressure sensitive paint data by singular value decomposition, *Measurement Science and Technology*, vol. 24, 075301 (7pp). doi:10.1088/0957-0233/24/7/075301

[27] Kameda M, Seki H, Makoshi T, Amao Y, Nakakita K (2008) Unsteady measurement of a transonic delta wing flow using a novel PSP, In: Proceedings of 26th AIAA Applied Aerodynamics Conference, AIAA 2008-6418. doi: 10.2514/6.2008-6418

[28] Nakakita K (2013) Detection of phase and coherence of unsteady pressure field using unsteady PSP measurement, In: Proceedings of AIAA Ground Testing Conference, AIAA-2013-3124. doi: 10.2514/6.2013-3124